

# Lawrence Berkeley National Laboratory

## Recent Work

### Title

Cation, Anion, and Radical Isomers of C<sub>4</sub>H<sub>4</sub>N: Computational Characterization and Implications for Astrophysical and Planetary Environments.

### Permalink

<https://escholarship.org/uc/item/9mw142xs>

### Journal

The journal of physical chemistry. A, 124(10)

### ISSN

1089-5639

### Authors

Hendrix, Josie  
Bera, Partha P  
Lee, Timothy J  
[et al.](#)

### Publication Date

2020-03-01

### DOI

10.1021/acs.jpca.9b11305

### Supplemental Material

<https://escholarship.org/uc/item/9mw142xs#supplemental>

Peer reviewed

# The Cation, Anion, and Radical Isomers of $C_4H_4N$ : Computational Characterization and Implications for Astrophysical and Planetary Environments

Josie Hendrix,<sup>\*,†</sup> Partha P. Bera,<sup>‡,¶</sup> Timothy J. Lee,<sup>‡</sup> and Martin Head-Gordon<sup>†</sup>

<sup>†</sup>*Department of Chemistry, University of California, Berkeley, CA, USA 94720*

<sup>‡</sup>*NASA Ames Research Center, Moffett Field, Mountain View, CA, USA 94035*

<sup>¶</sup>*Bay Area Environmental Research Institute, Moffett Field, Mountain View, CA, USA 94952*

E-mail: josie\_hendrix@berkeley.edu

## Abstract

Nitrogen-containing ions and molecules in the gas phase have been detected in non-Earth environments such as dark molecular clouds, and more recently in the atmosphere of Saturn's moon Titan. These molecules may serve as precursors to larger heterocyclic structures that provide the foundation of complex biological molecules. On Titan, molecules of  $m/z$  66 have been detected by the Cassini mission, and species of the empirical formula  $C_4H_4N$  may contribute to this signature. We have characterized seven isomers of  $C_4H_4N$  in anionic, neutral radical, and cationic states using density functional theory. Structures were optimized using the range-separated hybrid  $\omega$ B97X-V with the cc-pVTZ and aug-cc-pVTZ basis sets. Anionic and radical  $C_4H_4N$  favor cyclic structures with aromatic and quasi-aromatic electron arrangements, respectively. Interestingly, ionization from the radical surface to the cation induces significant changes in structural stability, and the global minimum for positively charged isomers is  $CH_2CCHCNH^+$ , a pseudo-linear species reminiscent of cyanoallene. Select formation pathways to these structures from Titan's existing or postulated gas-phase species, reactions which are also relevant for other astrophysical environments, are discussed. By characterizing  $C_4H_4N$  isomers, we have identified energetically stable anionic, radical, and cationic structures that may be present in Titan's atmosphere and dark molecular clouds.

## Introduction

The emergence of biomolecules on early Earth is an intriguing topic and the chemical origins of life have not been fully resolved. Groundbreaking experiments performed by Miller in the mid-1950's under reducing conditions showed that complex organic molecules can form from small inorganic precursors in the presence of electric discharge<sup>1</sup>, supporting the possibility of biomolecule formation in the atmosphere of primitive Earth. Since this iconic experiment,

our understanding of chemistry in early Earth environments has continued to grow, and multiple synthetic routes leading to complex organic species have emerged<sup>2-11</sup>.

Though these complex molecules have been shown to form without pre-existing complex organic material, the particular atmospheric conditions of our young planet are not entirely certain. Thus, it is important to consider a variety of alternative conditions supporting biomolecule origin.

Exogenous delivery of key precursors to Earth

from extraterrestrial environments is one example. Complex organic molecules have been found in many astrophysical environments including interstellar molecular clouds, protoplanetary nebulae, and primitive solar system bodies<sup>12</sup>. Particularly, the existence of these molecules (including pristine amino acids and sugars) has been confirmed in meteoritic samples of extraterrestrial origin<sup>13-16</sup>, implying that exogenous delivery of organic molecules during or after the formation of the solar system is a viable pathway that could have precluded biomolecule formation on early Earth, and potentially contributed to the origins of life on this planet. Direct formation of these nucleobases on interstellar cold grains has been shown to occur when ices containing the appropriate precursors undergo UV irradiation<sup>17-22</sup>. Additionally, these compounds could be synthesized in the gas phase and condense onto cold grains for delivery to early planetary systems.

Gas-phase reactions are more likely to occur in environments such as the circumstellar envelopes of dying stars, dark molecular clouds, and select planetary atmospheres where particle densities are higher than in the diffuse interstellar medium<sup>23-25</sup>. As well as illuminating formation pathways to complex species that could be delivered exogenously to Earth through meteorites, some of these processes serve as useful templates when considering the atmospheric conditions of early Earth. Low temperatures typical of these environments disfavor particle growth through neutral-neutral reactions between closed-shell members, which require large activation barriers; however, reactions involving radicals and ions proceeding through small or submerged energetic barriers have been shown to produce complex nitrogen-containing molecules<sup>26-29</sup>. Ion-molecule chemistry between atomic nitrogen and cyclic precursors can generate nitrogenated polycyclic aromatic hydrocarbons (PAH)<sup>30,31</sup>, and cyclization reactions of smaller nitrogenated and hydrocarbon species are also quite possible<sup>25,32</sup>.

A planetary body of particularly rich nitrile chemistry is the ionosphere of Titan, Saturn's moon. Titan's dense atmosphere, composed primarily of nitrogen (94 - 98%) and methane

(1.8 - 6.0%)<sup>33</sup>, is exposed to UV and extreme-UV radiation as well as energetic electrons from Saturn's magnetosphere<sup>33</sup>; this particular combination favors molecular interactions involving and producing nitrogen-containing molecules. Understanding processes occurring in Titan's atmosphere that could lead to complex nitrogenated organics is important for species identification both here and in molecular clouds, and these may mimic reactions that took place in a primitive Earth environment.

The recent Cassini-Huygens mission, equipped with an ion neutral mass spectrometer (INMS), performed a fly-by of Titan and collected data on neutral, cationic, and anionic species up to several hundred daltons in size<sup>34-38</sup>. Accurate identification of new nitrogen-containing species in remote environments such as the atmosphere of Titan is experimentally difficult, and often relies on theoretical groundwork when existing molecular information is limited. Here, we explore the lower mass end of the INMS readings (<100 daltons), and specifically direct our investigation to the measured signal at  $m/z$  66<sup>39-42</sup>. There are several stoichiometries that could potentially contribute to this mass peak (e.g.  $C_4H_4N$ ,  $C_2N_3^-$ ,  $C_5H_6^+$ ,  $C_3H_2N_2$ , etc.<sup>42,42-45</sup>), belonging to hydrocarbons or nitriles due to the atmospheric composition. We choose to focus our attention on isomers of the empirical formula  $C_4H_4N$  due to its potential to form heterocyclic ring structures.

Similar characterizations of  $C_4H_5N$  and  $C_4H_3N$  isomers have been performed to identify energetically favorable arrangements<sup>46,47</sup>. For example,  $C_4H_5N$  is by far most stable in ring form as pyrrole<sup>47</sup>. This aromatic 5 membered ring contains  $6\pi$  electrons; the apical nitrogen is  $sp^2$  hybridized in the molecular plane, leaving its lone pair to delocalize into the aromatic system. Linear species of  $C_4H_3N$  (isomers of which have been detected in the interstellar medium<sup>48-50</sup>) have been studied by Custer et al.<sup>46</sup>, who found that methylcyanoacetylene  $CH_3CCCN$  was the most stable isomer of those tested. The preferred structures of each chemical formula are good indicators of which isomers are most likely to be present in cold extrater-

restrial environments.

Changes in the electronic structure of these molecules influence isomer stability and reactivity. Multiple potential energy surfaces are available to  $C_4H_4N$  depending on the mechanism of formation: anionic or neutral radical species may form via deprotonation or dehydrogenation of cyclic  $C_4H_5N$ , while protonation of  $C_4H_3N$  leads to cationic  $C_4H_4N^+$ . In the open-shell radical or closed-shell ionic form, molecules such as  $C_4H_4N$  are especially reactive and could initiate reactions producing the larger heterocyclic structures that compose biomolecules. Reactions involving pyrrole and pyridine (the six-membered aromatic analog) have been experimentally probed in this vein<sup>26,27,51</sup>.

Because chemistry in cold extraterrestrial environments is driven primarily by radical-radical and ion-radical reactions (as well as those between a closed shell species and an ion or radical), characterization of  $C_4H_4N$  in different electronic states will help us identify which species are likely to participate in pathways leading to biologically relevant molecules. Thus, we present a systematic exploration of select  $C_4H_4N$  isomers in their cationic, anionic, and radical forms. The relative stability of these structures in each electronic state is discussed, as well as select formation routes via the uni-molecular or bi-molecular reactions of available species. By characterizing  $C_4H_4N$ , we produce structures that will narrow the field of candidate molecules that may contribute to the observed mass data from Cassini INMS, and thus help guide the identification of new species. In the process, we hope to also gain a better understanding of how unique cationic, anionic, or radical isomers are formed and could contribute to the synthesis of complex organics. This will help us understand not only processes occurring in the rich atmosphere of Titan or that of early Earth, but also in cold molecular clouds where nitrogen-containing molecules may form in the gas phase and deposit onto the cold grains of meteorites for delivery to planetary bodies.

## Methods

Seven isomers of  $C_4H_4N$  (see Figure 3 for optimized radical structures, which deviated the least from starting geometries) were chosen based on their presence in both the chemical physics and combustion literature<sup>47,52–54</sup>. Though we recognize that these seven isomers are not fully representative of all possible configurations, the number of species was limited to likely low-energy structures to lessen computational cost and focus on adequate characterization of individual species. Full geometry optimizations were performed for structures of all seven isomers and several relevant precursors using unrestricted density functional theory (DFT), a widely used method for quantum mechanical calculations by virtue of its impressive accuracy at low computational cost. Our DFT calculations were performed on an ultra-fine integration grid of 99 radial points and 590 angular points. Optimizations of starting structures A-G were performed using the  $\omega$ B97X-V functional<sup>55</sup>. The range-separated hybrid  $\omega$ B97X-V has been shown to out-perform many other existing functionals for calculations on numerous relevant systems<sup>56–59</sup>. Inclusion of range-separation helps mitigate the infamous 'self-interaction error' inherent to DFT, which can lead to inaccuracies in energetics, especially in radical systems such as the ones studied here<sup>60,61</sup>. Each structure was allowed to relax from the initial geometry on the appropriate potential energy surface: anion, neutral radical, and singlet cation. Isomers are referred to by distinguishing letter and charge symbol hereafter (e.g.  $A^-$ ,  $A^\bullet$ , and  $A^+$  for anionic, neutral radical, and cationic isomer A).

Cationic and radical isomers were optimized with  $\omega$ B97X-V in the cc-pVTZ basis. Because the use of diffuse functions is generally recommended for DFT calculations involving anions, anionic structures were optimized using the larger aug-cc-pVTZ basis set. Inclusion of sufficient diffuse functions in aug-cc-pVTZ better captures the 'tail behavior' of atomic orbitals farther from the atom's nucleus, a crucial feature for structures with excess electron density<sup>62</sup>. Natural Population Analyses<sup>63</sup> were calculated using  $\omega$ B97X-V in aug-cc-pVTZ. To confirm that the equilibrium geometries of the

isomers were indeed minima and obtain zero point energies, vibrational frequency analyses were performed for cations and radicals at the  $\omega$ B97X-V/cc-pVTZ level, and for anions at the  $\omega$ B97X-V/aug-cc-pVTZ level. Vibrational constants and intensities are provided in the Supplemental Information. Because the accuracy of the isomer energies was crucial for the purposes of this study, single-point energies were calculated for isomers A-G of the cation, radical, and anion at the coupled cluster level, including up to triple excitations using CCSD(T)<sup>64</sup>. In conjunction with second-order Møller-Plesset perturbation theory with the resolution of the identity approximation (RI-MP2)<sup>65,66</sup> in progressively larger basis sets, energies were extrapolated to the complete basis set limit (CBS) using the following scheme:

$$E(CCSD(T)/CBS) = E(HF/cc-pV5Z) + E^{corr}(RI-MP2/CBS_{3,4,5}) + E^{corr}(CCSD(T)/cc-pVTZ) - E^{corr}(RI-MP2/cc-pVTZ) + ZPE(\omega B97X-V/cc-pVTZ)$$

Here, the  $E^{corr}(RI-MP2/CBS_{3,4,5})$  term contains the complete basis extrapolation using cc-pVTZ through cc-pV5Z:

$$E^{corr}(RI-MP2/cc-pVNZ) = E^{corr}(RI-MP2/CBS_{3,4,5}) + AN^{-3}$$

The variable  $N$  corresponds to the basis set cardinal number<sup>67</sup>, which here is 5. For anionic structures, the same scheme was followed using aug-cc-pVNZ.

In exploring potential formation pathways of the lowest-energy structures, the freezing-string method was utilized to generate a guess for transition state structures<sup>68</sup>. Once a suitable transition state was located, its initial structure and Hessian were further improved using the partitioned-rational function optimization eigenvector following method<sup>69</sup>. All this is done using  $\omega$ B97X-V with cc-pVTZ.

All calculations were performed using the Q-Chem 5 software package<sup>70</sup>.

## Structural Results and Discussion

### Anionic isomers

Figure 1 shows the energetic ordering of structures on the closed-shell anionic potential energy surface.



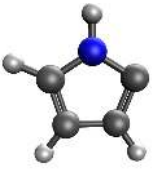




Isomer (Formula)	Structure	Relative Energy
A <sup>-</sup> (c-C <sub>4</sub> H <sub>4</sub> N)		0.00
E <sup>-</sup> (CH <sub>3</sub> CCHCN)		36.01
B <sup>-</sup> (c-C <sub>α</sub> C <sub>3</sub> H <sub>3</sub> NH)		36.50
D <sup>-</sup> (CH <sub>2</sub> CCH <sub>2</sub> CN)		45.38
C <sup>-</sup> (c-C <sub>β</sub> C <sub>3</sub> H <sub>3</sub> NH)		47.28
F <sup>-</sup> (CH <sub>2</sub> CCHCNH)		58.77
G <sup>-</sup> (CH <sub>2</sub> CHCCHN)		88.29

Figure 1: Structures of C<sub>4</sub>H<sub>4</sub>N in the closed-shell anionic state. Isomer (A<sup>-</sup>) was found to be the energetic minimum, stabilized by a favorable 6 $\pi$  aromatic electron arrangement. Energetic differences are calculated with respect to (A<sup>-</sup>) in kcal/mol.

The energetic differences of the anionic isomers were computed with respect to cyclic iso-

mer ( $A^-$ ), which was found to be the most stable structure (energetic minimum). Electronically, ( $A^-$ ) is isoelectronic to pyrrole. Pyrrole and  $C_4H_4N^-$  are aromatic heterocycles, each with a total of  $6\pi$  electrons; four  $\pi$  electrons are contributed by carbon atoms in the conjugated 5-member ring, and the remaining two are donated from the nitrogen’s lone pair.

In neutral pyrrole, the nitrogen atom has an in-plane trigonal configuration, bonding to the surrounding  $\alpha$  carbons and a single hydrogen; the remaining lone electron pair occupies  $2p_z$  out-of-plane, contributing to the  $6\pi$  aromatic ring system<sup>71</sup>. Deprotonation of pyrrole occurs at the apical nitrogen, as the electronegativity difference between N and H makes this proton the most acidic. In the anionic  $C_4H_4N$  (structure ( $A^-$ )), the aromatic configuration is retained. Due to this favorable electronic arrangement, isomer ( $A^-$ ) is by far the favored structure on the anionic surface - the second lowest energy structure ( $E^-$ ) lies 36 kcal/mol above ( $A^-$ ) in energy and is quasi-linear, stabilized by several resonance structures. Most of the negative charge in ( $E^-$ ) is localized on the carbon at which the molecule sharply bends; because of ( $E^-$ )’s shape, electron density centered on this carbon is spatially separated from the lone electron pair on nitrogen, decreasing steric interactions between the respective electron clouds. To the point, cyclic ( $B^-$ ) (deprotonated at the  $\alpha$  carbon) is slightly destabilized by comparison; steric interactions between electrons on the alpha carbon and the adjacent nitrogen are comparatively unfavorable.



Figure 2: Bond lengths (**I.**) and Natural charges (**II.**) for anionic ( $A^-$ ) calculated in  $\omega$ B97X-V/aug-cc-pVTZ. Charges indicated on carbon atoms are a sum of the C–H moiety. The aromatic nature of the ring leads to a planar structure with lengthened  $C_\alpha=C_\beta$  and slightly shortened  $C_\beta-C_\beta$  and  $C_\alpha-N$  (compared to pyrrole).

Figure 2 shows bond lengths (**I.**) and Natural charges (**II.**) in anionic isomer ( $A^-$ ), the global minimum for this set. The  $6\pi$  aromatic conjugation of the structure results in a shortened 1.416 Å  $C_\beta-C_\beta$  (vs 1.424 Å), a lengthened 1.397 Å  $C_\alpha=C_\beta$  (vs 1.371 Å), and shortened 1.357 Å  $C_\alpha-N$  (vs 1.370 Å) bond (compared to those in neutral pyrrole), culminating in a planar structure with  $C_{2v}$  symmetry. These slight deviations from parent pyrrole (optimized at the same level of theory) are due largely to the extra electron density of the anionic lone pair atop the apical nitrogen, which also drives the  $109.7^\circ$   $C_\alpha-N-C_\alpha$  angle in pyrrole to a more acute  $105.0^\circ$  in deprotonated ( $A^-$ ). Natural charges reflect the spread of electron density across the ring, with negative charge centered mostly at nitrogen as expected, but also distributed in a good proportion to the  $\beta$  carbons.

Structural stability depends highly on the deprotonation site in the anionic  $C_4H_4N$  cyclic isomers. Deprotonation of the heteroatom to form ( $A^-$ ) is clearly the most favorable process - as discussed previously, the distinct difference in electronegativity along the N–H bond makes this proton highly acidic. Deprotonation at an  $\alpha$  or  $\beta$  carbon in the ring is comparatively more difficult, despite the similarities in N–H and C–H bond enthalpies (both 338 kJ/mol<sup>72</sup>). Structures ( $B^-$ ) and ( $C^-$ ) (with C–H bond cleavage at  $\alpha$  and  $\beta$  sites, respectively) lie over 36 kcal/mol higher in energy than ( $A^-$ ). Deprotonation at the  $\alpha$  carbon in ( $B^-$ ) is preferred over a similar process at the

$\beta$  site in ( $C^-$ ), with the latter relatively destabilized by just over 11 kcal/mol. In general, electrophilic substitutions to five-member heterocyclic rings favor attack at the  $\alpha$  carbon. Compared to the  $\beta$  site, substitution at the  $\alpha$  carbon leads to a greater number of intermediate resonance structures, allowing for more facile charge delocalization and a more stabilized product<sup>73</sup>. Due to this effect and the proximity of the electron-withdrawing heteroatom, the hydrogen atom at the  $\alpha$  carbon is more acidic than that at the  $\beta$  carbon, favoring  $\alpha$  deprotonation of the cycle. These effects stabilize ( $B^-$ ) relative to ( $C^-$ ).

### Radical isomers

For the radical electronic configuration, ( $A^\bullet$ ) is once again found to be the global minimum as shown in Figure 3. Interestingly, quasi-linear isomer ( $E^\bullet$ ) is quite close in energy to cyclic radical isomers ( $B^\bullet$ ) and ( $C^\bullet$ ); these isomers all lie  $\sim 23$ - $26$  kcal/mol above ( $A^\bullet$ ) in energy. The relative energetics of isomers ( $B^\bullet$ ) and ( $C^\bullet$ ) with respect to ( $A^\bullet$ ) indicate that the location of the radical electron influences heterocycle stability. Other linear and semi-linear isomers of  $C_4H_4N$  are found to be subsequently higher in energy than their cyclic counterparts on the radical PES, though with energetic differences less dramatic than in the anionic case.






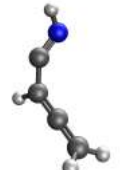

Isomer (Formula)	Structure	Relative Energy
$A^\bullet$ (c- $C_4H_4N$ )		0.00
$C^\bullet$ (c- $C_\beta C_3H_3NH$ )		23.55
$B^\bullet$ (c- $C_\alpha C_3H_3NH$ )		24.22
$E^\bullet$ ( $CH_3CCHCN$ )		26.65
$D^\bullet$ ( $CH_2CCH_2CN$ )		30.67
$F^\bullet$ ( $CH_2CCHCNH$ )		46.73
$G^\bullet$ ( $CH_2CHCCHN$ )		56.42

Figure 3: Structures of  $C_4H_4N$  in the radical configuration; relative energies are calculated with respect to ( $A^\bullet$ ) in kcal/mol. Similar to the anionic state, ( $A^\bullet$ ) is the lowest energy structure. Though electron removal has resulted in loss of complete aromaticity, ( $A^\bullet$ ) still benefits from some delocalization of the remaining  $5\pi$  electrons over the ring.

Recent calculations performed by Sah et al. on a variety of five-membered heterocyclic species found that radicals centered at the heteroatom were favored over those located on nearby  $\alpha$  or  $\beta$  carbon atoms - unpaired electrons on heteroatoms can delocalize across the  $\pi$  orbitals of the ring more easily<sup>52</sup>. For dehydrogenated pyrrole species ( $C_4H_4N$ ), these authors optimized heteroatom,  $\alpha$  carbon, and  $\beta$

carbon centered radicals (corresponding to our ( $A^\bullet$ ), ( $B^\bullet$ ), and ( $C^\bullet$ )) at several levels of theory, and our computed energetic differences are in good agreement.

The particular stability of ( $A^\bullet$ ) can be rationalized in a way similar to the anionic analog. Recall the nature of the apical nitrogen - in both pyrrole and the aforementioned anionic counterpart, N is  $sp^2$  hybridized and maintains a trigonal configuration within the molecular plane. In anionic ( $A^-$ ), nitrogen has two electron pairs. One occupies the  $2p_y$  orbitals to maintain the  $sp^2$  arrangement, and the other resides in  $2p_z$  out of the molecular plane, contributing to the aromatic ring system. ( $A^-$ ) is isoelectronic to cyclopentadienyl anion, which has degenerate  $\pi$  molecular orbitals due to the  $D_{5h}$  symmetry of the molecule<sup>74</sup>. However, inclusion of a nitrogen atom in the ring reduces the overall symmetry to  $C_{2v}$  in pyrrole and ( $A^-$ ), and the  $\pi$  orbitals are no longer energetically degenerate<sup>75</sup>. Due to their hybridization and non-participation in the  $\pi$  system, nitrogen's  $2p_y$  orbitals lie lower in energy than the  $2p_z$  orbitals. Because of this, electron removal from ( $A^-$ ) to form the radical ( $A^\bullet$ ) occurs from  $2p_z$  - this disturbs the aromaticity of the cycle, but the radical electron can still delocalize over the ring, resulting in a pseudo-aromatic  $5\pi$  arrangement. Considering the stabilization of  $2p_y$  and the observation that ( $A^\bullet$ ) suffers no distortion from the x-y plane, it is reasonable to assert that the unpaired electron of the radical occupies  $2p_z$  and the lone pair of  $2p_y$  remains intact.

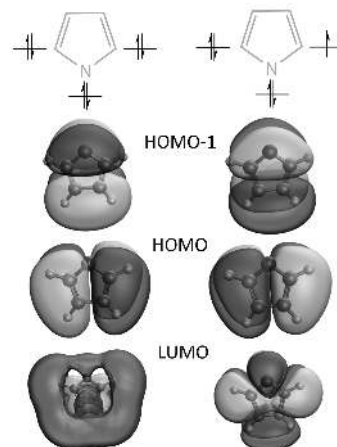


Figure 4: Comparison of molecular orbitals and electron configuration between ( $A^-$ ) (left) and ( $A^\bullet$ ) (right). The HOMO of anionic ( $A^-$ ) is similar to the SOMO of the corresponding radical species, indicating electron removal from the anionic occurs from  $2p_z$  orbitals on nitrogen that contribute to the  $\pi$  system. The  $2p_y$  orbitals are largely undisturbed and contribute to the planarity of ( $A^\bullet$ ).

The orbitals shown in Figure 4 support this picture. The highest occupied molecular orbital (HOMO) of anionic ( $A^-$ ) and singly occupied molecular orbital (SOMO) of radical ( $A^\bullet$ ) show similar shapes, indicating a similar contribution from the atomic orbitals.

The molecular orbitals of these heterocycles and their occupations have been previously appraised; Gianola et al. investigated the electronic structure of pyrrolide anion and its corresponding radical in detail, noting the clear bonding character between  $\alpha$  and  $\beta$  carbons<sup>75</sup>. In our systems, this interaction is particularly strong in the anion, and removal of an electron to form the radical reduces bonding character. This manifests as a slight lengthening of the central  $C_\alpha=C_\beta$  bonds highlighted in Figure 5. Though these structural changes occur due to the loss of aromaticity in radical ( $A^\bullet$ ), decreased interaction between  $\alpha$  and  $\beta$  carbons does not completely destabilize the ring.



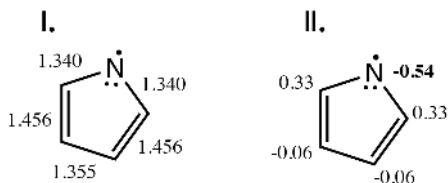


Figure 5: Bond lengths (**I.**) and Natural charges (**II.**) for radical ( $A^\bullet$ ) calculated in  $\omega$ B97X-V/cc-pVTZ. Charges indicated on carbon atoms are a sum of the C–H moiety. Electron removal from anionic ( $A^-$ ) has disrupted the aromaticity of the heterocycle, inducing small structural changes in the radical and reflecting the depletion of bonding character between  $\alpha$  and  $\beta$  carbons.

Figure 5 shows the bond lengths (**I.**) and Natural charges (**II.**) of isomer ( $A^\bullet$ ) in the radical configuration. Though ( $A^\bullet$ ) is pseudo-aromatic and stabilized on the radical surface, the loss of complete aromaticity is reflected in the bond lengths and charge distribution.

Stretching and shortening of bonds in radical ( $A^\bullet$ ) reflects fluctuations of electron density. Compared to anionic ( $A^-$ ), there is a slight lengthening of the 5-member heterocycle, as the  $C_\alpha=C_\beta$  bonds stretch by  $0.059 \text{ \AA}$  while  $C_\alpha-N$  and  $C_\beta-C_\beta$  shorten by  $0.017$  and  $0.061 \text{ \AA}$  respectively.

While the loss of bonding character between  $\alpha$  and  $\beta$  carbons manifests in  $C_\alpha=C_\beta$  lengthening, the apical  $C_\alpha-N-C_\alpha$  angle remains nearly unaltered from the aromatic anion ring at  $104.6^\circ$ , indicating that the position of the lone pair atop N remains undisturbed and providing further support for the proposed  $5\pi$  electronic arrangement.

As shown in Figure 5 **II.**, charge differences between ring atoms have become more pronounced than in the anionic case of ( $A^-$ ). These changes in charge distribution go hand-in-hand with the altered bond lengths. Stretching of  $C_\alpha=C_\beta$  in ( $A^\bullet$ ) brings the p orbitals of the  $\alpha$  carbons closer to nitrogen, donating some of their electron density to the more electronegative atom. As a consequence,  $\alpha$  carbons have taken on a noticeable positive charge, and are quite charge separated from their neighboring nitrogen.

The  $\beta$  carbons of ( $A^\bullet$ ) pull closer together at

a distance nearing that of a carbon-carbon double bond. Like the  $\alpha$  carbons,  $\beta$  carbons have become more positive than nitrogen (by  $0.48$  charge units, versus their  $0.36$  charge unit difference in ( $A^-$ )). Though the effect is less drastic,  $\alpha$  and  $\beta$  carbons themselves are charge separated to a greater degree as bonding character between them decreases.

Additionally, spin density delocalization contributes to the stability of ( $A^\bullet$ ) and helps explain the relative stabilities of cyclic isomers ( $B^\bullet$ ) and ( $C^\bullet$ ). As shown in Figure 3, there is a  $\sim 24$  kcal/mol difference in energy between ( $A^\bullet$ ) and the other cyclic isomers, though ( $B^\bullet$ ) and ( $C^\bullet$ ) less than  $1$  kcal/mol apart. This is in contrast to anionic ( $B^-$ ) and ( $C^-$ ) isomers, which were energetically separated by about  $11$  kcal/mol (with relative stabilization of ( $B^-$ )).

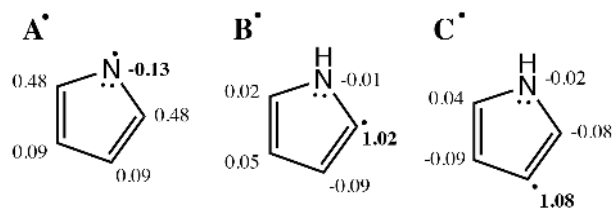


Figure 6: Spin densities calculated for isomers ( $A^\bullet$ ), ( $B^\bullet$ ), and ( $C^\bullet$ ). Electron spin is relatively delocalized in ( $A^\bullet$ ), while it is highly localized for ( $B^\bullet$ ) and ( $C^\bullet$ ).

For dehydrogenation reactions of pyrrole to form the radical, acidity of the departing hydrogen is less predictive of the preferred reaction site than it is for deprotonation reactions; since isomers ( $A^\bullet$ ), ( $B^\bullet$ ), and ( $C^\bullet$ ) are carrying a radical electron, spin densities help explain some of the observed stability trends, shown in Figure 6. Highly localized electron spin results in a very reactive species, while delocalized spin conversely stabilizes a structure<sup>52</sup>. Figure 6 shows the distribution of spin between the two  $\alpha$  carbons in ( $A^\bullet$ ), contributing to the stability of the structure. Conversely, ( $B^\bullet$ ) and ( $C^\bullet$ ) show highly localized spin densities at their respective dehydrogenation sites, and spin is localized to the same degree in each, so  $\alpha$  dehydrogenation is not particularly favored over the  $\beta$  site, and vice versa.

## Cationic isomers

Removal of another electron from the  $C_4H_4N$  radical surface results in the singlet cationic electronic configuration. Ionization is accompanied by more major shifts in the stability ordering of these isomers shown in Figure 7.








Isomer (Formula)	Structure	Relative Energy
$F^+$ ( $CH_2CCHCNH$ )		0.00
$G^+$ ( $CH_2CHCCHN$ )		23.91
$A^+$ ( $c-C_4H_4N$ )		25.83
$C^+$ ( $c-C_\beta C_3H_3NH$ )		32.95
$B^+$ ( $c-C_\alpha C_3H_3NH$ )		34.81
$E^+$ ( $CH_3CCHCN$ )		40.25
$D^+$ ( $CH_2CCH_2CN$ )		40.62

Figure 7: Structures of  $C_4H_4N$  in the cationic state; relative energies are expressed in kcal/mol. Heterocyclic (A), the global minimum on both anionic and radical potential energy surfaces, is now reduced to an anti-aromatic arrangement with  $4\pi$  electrons in the ring, destabilizing the structure. The global minimum for the cationic surface was found to be ( $F^+$ ), a linear structure reminiscent of cyanoallene.

Previously, cyclic (A) was found to be the global minimum on the radical and anionic potential energy surfaces; however, in the cationic

case, ( $G^+$ ) and ( $F^+$ ) are found to be lower in energy. Similar to the anion/radical transition, transition from radical ( $A^\bullet$ ) to the cation can occur via electron removal from either the  $2p_y$  or  $2p_z$  of nitrogen, and once again this removal occurs from the higher energy  $2p_z$  orbitals. Nitrogen's lone pair continues to occupy  $2p_y$  and planarity is retained; however, ( $A^+$ ) is now left relatively higher in energy due to its anti-aromatic  $4\pi$  electron arrangement.

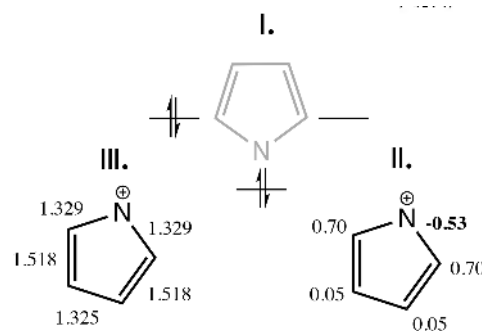


Figure 8: Electronic configuration (**I.**), Natural charges (**II.**), and bond lengths (**III.**) for cationic ( $A^+$ ). Charges indicated on carbon atoms are a sum of the C–H moiety. Half-filled orbitals contribute to the destabilization of this structure.

In response, the  $C_\alpha=C_\beta$  bonds elongate to 1.518 Å, close to a typical C–C single bond.

Cationic ( $A^+$ ) was found to be a transition state structure, and the now half-filled molecular orbitals (Fig. 8 **I.**) contribute to structural distortion that lowers the overall energy of the molecule. Despite its stretched and strained structure, the singlet cation was found to be lower in energy than the triplet configuration, though the singlet-triplet gap is small ( $\sim 5.2$  kcal/mol).

As shown in Figure 8 **III.**, the  $C_\alpha=C_\beta$  bonds have lengthened significantly compared to aromatic pyrrole or anionic ( $A^-$ ), approaching the length one would expect from a C–C single bond. Since ( $A^+$ ) is now antiaromatic, the bonding character between  $\alpha$  and  $\beta$  carbons established for anionic and radical species<sup>75</sup> is disrupted completely. Similar phenomena have been discussed in detail for the isoelectronic cyclopentadienyl cation<sup>74,76</sup>, another planar  $C_{2v}$  ring with modes of distortion leading

to lower symmetry (more energetically stable) structures<sup>77</sup>.

The stabilization of ( $G^+$ ) compared to ( $A^+$ ) is slightly surprising - however, structural strain within the three-membered ring is mitigated by electron delocalization, as the ring is aromatic by the  $4n+2$  rule, where here  $n=0$ . In isoelectronic 3-membered carbocations such as cyclopropenyl, structures are stabilized by delocalization of the  $2\pi$  electrons residing in the ring system, which can spread into empty  $2p$  orbitals of the positively charged carbon atoms<sup>78,79</sup>. Azirinylium cation, a three-membered ring with an apical nitrogen atom, has recently been investigated in the interstellar context and was found to be the most stable structural isomer of the formula  $C_2H_2N^+$ <sup>80</sup>.

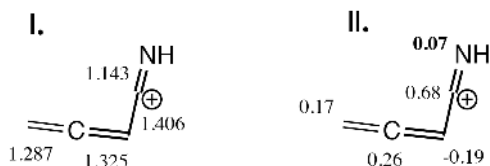


Figure 9: Bond lengths (**I.**) and Natural charges (**II.**) for cationic ( $F^+$ ). Charges indicated on carbon atoms are a sum of the  $C-H$  moiety. This carbocation is of  $C_s$  symmetry, and is stabilized by electronic donation from the neighboring nitrogen and  $C-H$   $\sigma$  bond to vacant  $p$  orbitals of the positively charged carbon.

The global minimum on the singlet cationic surface was found to be ( $F^+$ ), a highly conjugated quasi-linear isomer with  $C_s$  symmetry. As shown in Figure 9, the unsaturated carbon participating in the  $C=N$  double bond ( $C_2$ ) carries most of the positive charge. Hyperconjugation and resonance contribute to the stability of this carbocation. The empty  $p$  orbital on  $C_2$  can accept electron density from the nearby  $C-H$   $\sigma$  bond; this stabilizing interaction results in a lower-energy electron occupancy versus the isolated positively charged  $p$  orbital. Structurally, this manifests as the slight shortening of the  $C_2-C_3$  single bond. Similarly, a non-negligible amount of electron density from the lone pair on nitrogen interacts with the  $C_2$  empty  $p$  orbital, again stabilizing the positively charged carbon

atom and shortening the  $C=N$  double bond to a length approaching that of a  $C\equiv N$  triple bond.

## Ionization energies and electron affinities

Table 1 shows the adiabatic electron affinities and ionization energies of all isomers studied here as compared to the radical form in units of eV. Unsurprisingly, electron attachment to radical ( $A^\bullet$ ) forming anionic ( $A^-$ ) is quite favorable, as this leads to  $6\pi$  electrons in the ring. Energetic stabilization through anion formation decreases with structural stability of the anionic isomer. Electron affinity for isomer ( $F^\bullet$ ) was not included in this table due to the significant structural rearrangement that occurs upon electron gain (See Figures 1 and 3 for comparison between the structures).

Table 1: Adiabatic electron affinities and ionization energies (eV) relative to the radical species for all isomers. Single point energies were calculated for the  $\omega B97X-V/cc-pVTZ$  optimized geometries using (CCSD(T)/CBS) for all isomers. All species (except perhaps  $G$ ) are stabilized by electron gain. Ionization of radical ( $A^\bullet$ ) requires significant energy, while ionization of radical ( $F^\bullet$ ) is markedly more feasible.

Isomer	EA	IE
A	2.21	9.20
B	1.68	8.54
C	1.18	8.48
D	1.57	8.51
E	1.80	8.67
F	—	6.05
G	0.83	6.67

An interesting trend has emerged regarding ionization states of isomer ( $F$ ). On the anionic surface, previously linear ( $F$ ) rearranges to adopt a central 3-membered ring, promoting delocalization of negative charge. These structural adaptations require significant energy. In contrast, ionization to the cationic state supports the original linear arrangement.

## Astrochemistry Implications

In the previous sections, we calculated low-energy structures of cationic, radical, and anionic isomers, providing a structural starting point for further identification of species that may be present in Titan’s atmosphere and elsewhere. Providing highly accurate rotational data using theoretical methods for use in conclusive species identification is a challenging prospect<sup>81,82</sup>. Though our goal in this work was not to provide such data, our accurate structures in conjunction with their vibrational frequencies and IR intensities may still be used for species identification in interstellar measurements. As an example, the SOFIA EXES instrument gathers spectra in the 4.5–28.3 $\mu\text{m}$  wavelength range<sup>83</sup>; for applications such as these, *ab initio* quantum mechanics would produce reliable data to match signals to molecules<sup>84–86</sup>. Because calculated vibrational frequencies and IR intensities in addition to molecular structures are thus useful to provide astronomers with a solid foundation for deconvoluting measurable ro-vibrational data for small molecules, we provide vibrational frequencies and intensities for the energetic minima of each  $\text{C}_4\text{H}_4\text{N}$  state in the SI.

Small nitrogen-containing molecules such as  $\text{C}_4\text{H}_4\text{N}$  may be found in molecular clouds or in the ionospheres of planetary bodies such as Titan, and perhaps even existed in the young atmosphere of our own Earth long ago. In Titan’s nitrogen-rich atmosphere, many energy sources are available to initiate the formation of radicals and ions, including short wavelength ultraviolet (UV) radiation, extreme ultraviolet radiation (EUV) and an energetic flux of electrons from Saturn’s magnetosphere<sup>33</sup>. Nitriles produced in the upper atmosphere through photochemistry involving  $\text{N}_2$  and  $\text{CH}_4$ <sup>87–89</sup> presumably combine through ion-neutral or radical chemistry to form more complex species, contributing to the organic haze surrounding this planetary moon<sup>90</sup>.

Here, we investigate several relevant formation pathways leading to ions of  $\text{C}_4\text{H}_4\text{N}$  and their preferred structures.

## Anion species

The Cassini-Huygens mission identified a number of nitrogen-containing anionic species in Titan’s atmosphere, including anions of this molecular weight ( $m/z = 66$ )<sup>42</sup>. Though cyclic species such as isomers (A), (B), and (C) have yet to be unambiguously observed in the gas phase, precursors such as pyrrole and other N-heterocycles have been detected as products in plasma-discharge, H-NMR, and other experiments performed in Titan-like conditions or on tholin mixtures<sup>91,92</sup>.

With these observations in mind, the presence of pyrrole ( $\text{C}_4\text{H}_5\text{N}$ ) in Titan’s haze (or elsewhere in the interstellar medium) cannot be discounted, and we thus consider the direct formation of anionic ( $\text{A}^-$ ) from this hydrogenated five member ring to be a viable possibility.

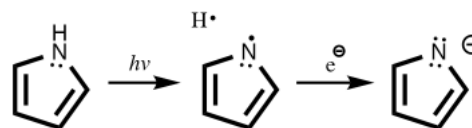


Figure 10: Formation of anionic ( $\text{A}^-$ ) from pyrrole via photodissociation. Dehydrogenation of the apical N follows excitation via energetic UV radiation, and electron attachment yields the stable anionic isomer.

Figure 10 depicts the formation of anionic ( $\text{A}^-$ ) through photodissociation of pyrrole and subsequent electron attachment. The photofragmentation and dynamics of excited state pyrrole have been extensively studied<sup>93–104</sup>(and references therein). Irradiation of ground state pyrrole ( $S_0$  ( $^1\text{A}_1$ )) at wavelengths from 238–250 nm (corresponding to photons of energy  $>4.8$  eV) excites the molecule into the  $^1\pi\sigma^*$  ( $^1\text{A}_2$ ) excited state from which hydrogen atoms are ejected quickly with high kinetic energy, yielding the ground state radical ( $\text{A}^\bullet$ )<sup>93,100,101</sup>; though this is formally electric-dipole forbidden, this mode intensifies by borrowing vibrational energy from higher energy states<sup>100,103</sup>. At shorter excitation wavelengths, ejection can also occur after direct excitation to the  $^1\pi\pi^*$  state ( $^1\text{B}_2$ ), which accesses the  $^1\pi\sigma^*$  ( $^1\text{A}_2$ ) energetic state via a conical intersec-

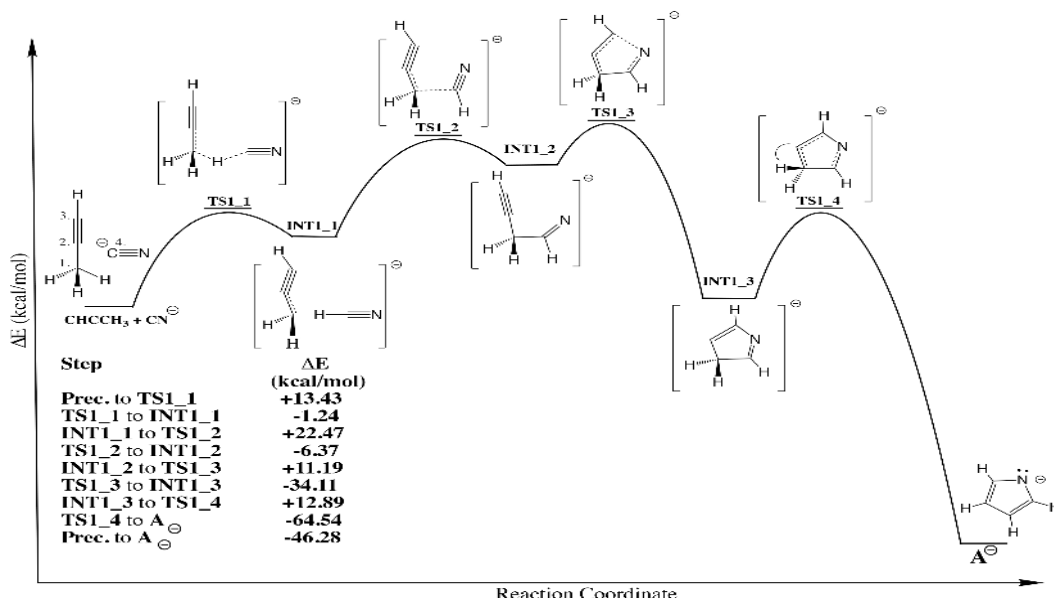


Figure 11: Schematic reaction path to anionic ( $A^-$ ) via  $CN^-$  and  $CH_3CCH$ . Both propyne and cyano anion have been detected in Titan's ionosphere, and could react to produce anionic ( $A^-$ ). However, the high energetic barriers to cyclization through this path are likely insurmountable without outside energetic input.

tion<sup>100,102</sup>. Slower hydrogen ejection can occur from a "vibrationally hot" pyrrole ground state  $S_0$ , where additional energy is dispersed to the many vibrational modes of the heterocycle<sup>100,101,103</sup>. In Titan's atmosphere, long wave UV radiation ( $>155$  nm) pierces down to intermediate altitudes (nearing 500 km), providing an adequate energy source for the photodissociation of pyrrole.

After formation of the ground state radical ( $A^\bullet$ ), the high electron affinity of this species (see Table 1) makes it a good candidate for thermal electron attachment. Processes such as radiative electron attachment (REA) have been investigated as a viable pathway to anion formation in Titan's atmosphere<sup>105</sup>. With many vibrational modes to disperse excess energy, ( $A^\bullet$ ) could efficiently form ( $A^-$ ) through this process, depicted in the second step of Figure 10. Additionally, the atmosphere is dense enough<sup>39</sup> to support third body interactions that may assist in diffusing the newly formed molecule's energy.

Alternatively, formation of anionic ( $A^-$ ) is possible through recombination of smaller species, such as  $CN^-$  and propyne ( $CHCCH_3$ ). Both precursors have been detected in molec-

ular clouds<sup>106,107</sup> and more recently in Titan's atmosphere: the signatures of various negative ions including  $CN^-$  were observed by Cassini-Huygens<sup>35,36</sup>, and several models calculate cyanide anion to be ubiquitous<sup>105</sup>. Heavier hydrocarbons including propyne have been detected at lower altitudes<sup>108</sup>.

Despite the availability of both of these species and the possibility of their reaction, our calculations have shown that the feasibility of this pathway is questionable; Figure 11 show that the reaction between  $CN^-$  and  $CHCCH_3$  passes through high barriers and would require significant energetic driving force. In this pathway, hydrogen shift from C1 of propyne to the C atom of  $CN^-$  (C4) and complexation of the two species requires  $>30$  kcal/mol in energy to proceed, even with the slight stabilization of INT1.1 after the hydrogen shift. Following this high entrance barrier to TS1.2, N attacks C3 in TS1.3 to form the cycle, and one more hydrogen shift from C1 to C2 (passing through a moderate barrier of  $\sim 13$  kcal/mol following stabilization of INT1.3) finally leads to the highly stabilized product, ( $A^-$ ). Despite the fact that anionic ( $A^-$ ) is stabilized by  $\sim 46$  kcal/mol compared to the reactants alone, cy-

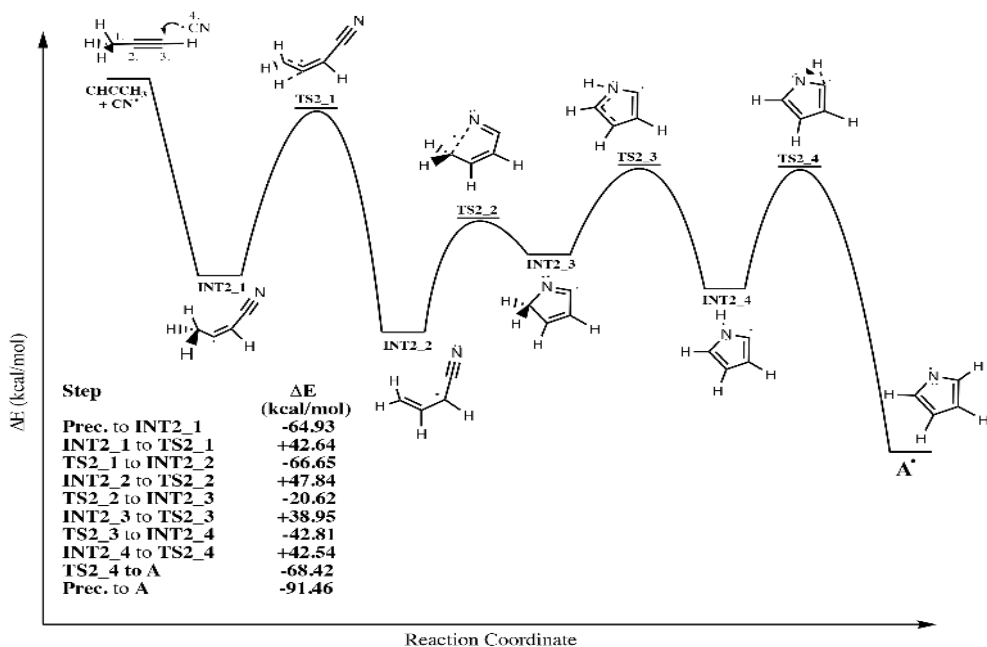


Figure 12: Schematic pathway to radical ( $A^*$ ) via  $CN^*$  and  $CH_3CCH$ . The presence of  $CN^*$  in Titan's ionosphere is predicted by several models to be significant. Cyclization of this radical and propyne proceeds barrierlessly to ( $A^*$ ), and thermal electron attachment to an intermediate or the product could result in ( $A^-$ ).

clization between  $CN^-$  and  $CHCCH_3$  appears to be difficult beginning from ground state reactants. To overcome the intermediate transition states, these two molecules would need to collide with a considerable amount of energy (which seems unlikely), or receive outside stimulation from photon absorption, as discussed for the process depicted in Figure 10.

Formation of anions such as ( $A^-$ ) through electron attachment to radical species is also possible. Reactions of radicals proceed rapidly through small or negligible barriers<sup>28</sup>, which is crucial in the cold environment of Titan's atmosphere or dense molecular clouds. Reactions of  $CN^*$  with propyne and other small hydrocarbons have been characterized experimentally and theoretically<sup>109</sup>, though heterocycle formation is not discussed in these works. In Figure 12, we have expanded the  $CN^*/CHCCH_3$  to include the possibility of cyclization.

Initial attack of  $CHCCH_3$  by  $CN^*$  leads to the highly stabilized intermediate INT2\_1, which has been previously characterized<sup>109</sup> and lies  $\sim 65$  kcal/mol below the initial reactants. Hydrogen shift from C1 to C2 to form INT2\_2 via

TS2\_1 passes through a seemingly tall barrier, but one that is still submerged below reactants by  $\sim 22$  kcal/mol. From INT2\_2, cyclization following N attack of C1 proceeds through TS2\_2, and the resulting structure (INT2\_3) is briefly stabilized before a subsequent hydrogen shift to form INT2\_4 (recognizable as ( $B^*$ )). Just one more adjacent shift of this hydrogen results in ( $A^*$ ), the global minimum on the radical surface, which is stabilized relative to reactants by  $\sim 91$  kcal/mol. Notably, unlike the reaction between  $CHCCH_3$  and  $CN^-$  forming the anionic ( $A^*$ ) (Fig. 11), energetic barriers encountered in the cyclization reaction involving  $CN^*$  are all submerged, making this formation pathway to ( $A^*$ ) feasible without outside stimulation. To move to the anionic surface, thermal electron attachment to an intermediate in the reaction pathway or the final product ( $A^*$ ) could lead to ( $A^-$ ) under appropriate conditions.

## Cationic species

Positively charged ions are also ubiquitous on Titan and in other extraterrestrial environ-

ments. The aforementioned energy sources (solar radiation and energetic electrons from Saturn’s magnetosphere) ionize  $N_2$  and  $CH_4$ , the main constituents composing the upper atmosphere. These ions react with neutrals to create a variety of charged hydrocarbon species.

Molecular mass data obtained during the fly-by of Titan includes traces linked to cations<sup>39-41</sup> - the mass peak appearing at  $m/z$  66 has been investigated by several models<sup>90,110</sup>, and is assigned by some to be  $CH_2CCHCNH^+$ , our isomer ( $F^+$ ). Because we found ( $F^+$ ) to be the global minimum cationic structure in our calculations, we propose that isomer ( $F^+$ ) is quite likely to contribute to this signal.

Cationic isomers of  $C_4H_4N$  such as ( $F^+$ ) could be interesting precursors to larger structures. As shown by values in Table 1, ionization to the cationic state requires significant energy, but sources of radiation are plentiful in this environment and ions are readily formed from their parent neutrals. Several potential reaction pathways have been included in models for cationic  $C_4H_4N$ .<sup>90,110</sup>

One likely formation route to ( $F^+$ ) is through protonation of allenyl cyanide (cyanoallene,  $CH_2C_2HCN$ ), which has been detected in the interstellar medium<sup>48</sup> and is predicted in Titan’s ionosphere. Isomers of the empirical formula  $C_3H_3N$  are most stable as methylcyanoacetylene ( $CH_3CCCN$ ), but cyanoallene ( $CH_2C_2HCN$ , direct precursor to ( $F^+$ )) only lies about 2.4 kcal/mol higher in energy<sup>46</sup>. This species has also been detected extraterrestrially near the Taurus Molecular Cloud (TMC-1)<sup>49,50</sup>.

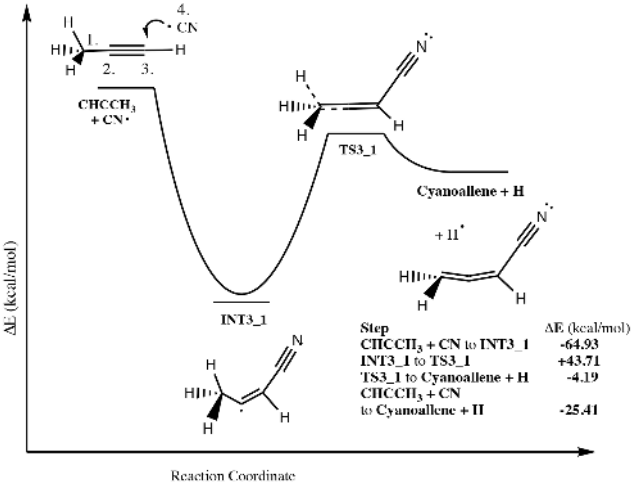


Figure 13: Schematic representation of cyanoallene formation via the reaction of propyne ( $CH_3CCH$ ) and cyano radical ( $CN^\bullet$ ). The relevant transition state has been characterized by Balucani et al. and occurs through a submerged energetic barrier. This reaction is exothermic by about 25 kcal/mol.

The formation of cyanoallene may occur through reactions between precursors discussed above, namely propyne ( $CH_3CCH$ ) and cyano radical ( $CN^\bullet$ ). The reaction of cyano radical with propyne has been investigated experimentally and theoretically<sup>111</sup>. Balucani et al. used a combination of crossed beam experiments and *ab initio* calculations to characterize products and transition states. Reaction of cyano radical with  $CH_3CCH$  to form products including  $CH_2CCHCN$  (cyanoallene) is barrierless and exothermic overall<sup>111</sup>. When examined at the  $\omega B97X-V/cc-pVTZ$  level of theory, the geometries and energetics of key structures along this reaction path (shown in Figure 13) are in good agreement with Balucani’s calculations.

Because the reaction depicted in Figure 13 is barrierless, it could feasibly occur in the cold environments of Titan’s atmosphere or molecular clouds. Formation of isomer ( $F^+$ ) ( $CH_2CCHCNH^+$ ) from cyanoallene would simply require protonation of the neutral species. Due to their high proton affinities, nitriles are good acceptors for  $H^+$ <sup>110</sup>.

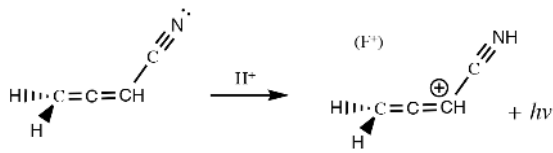


Figure 14: Protonation of cyanoallene to form isomer ( $F^+$ ). The excess energy may be emitted as a photon, or dispersed via collisions with a third body in the dense atmosphere of Titan. Structures were here optimized at the  $\omega$ B97X-V/aug-cc-pVTZ level of theory.

Figure 14 shows the protonation of cyanoallene to form isomer ( $F^+$ ). Cyanoallene has a high proton affinity (over 8eV). Excess energy resulting from this process could be emitted as a photon from isomer ( $F^+$ ), or be dispersed through third body interactions in the dense atmosphere of Titan.

## Conclusions

In this work, we have investigated isomers of  $C_4H_4N$  in cationic, neutral radical, and anionic states to determine the structures of  $C_4H_4N$  that could be present in Titan’s atmosphere or in molecular clouds. We found the energetic ordering of isomers to change with electronic state; that is, the most stable structures for anionic isomers were different from those same configurations on the cationic PES. For anionic species, the global minimum was found to be ( $A^-$ ). This cyclic isomer, analogous in structure to deprotonated pyrrole, is an aromatic ring containing six  $\pi$  electrons. Negative charge is well distributed between the electronegative nitrogen atom and  $\beta$  carbons of the ring. On the radical PES, ( $A^\bullet$ ) remains the most stable isomer, preserving a quasi-aromatic five  $\pi$  arrangement after electron removal from the anion. Lengthening of the central  $C_\alpha=C_\beta$  bonds occurs as bonding character between  $\alpha$  and  $\beta$  carbons decreases. Electron density again centers on the apical nitrogen and  $\beta$  carbons, though charge discrepancy between ring members is more pronounced.

Upon ionization to the cationic state, structural trends in stability present for anionic and radical isomers change notably. Previously

stable ( $A$ ) now has only four  $\pi$  electrons in the cationic ring, creating an unfavorable anti-aromatic arrangement. In contrast to the anionic and radical species, linear isomer ( $F^+$ ) was found to be the global minimum on the cationic surface. Hyperconjugation contributes to the stability of this structure, and the terminal nitrogen can donate electron density into empty p orbitals of the carbocation.

( $A$ ), the most stable  $C_4H_4N$  isomer of those studied here for anions and radicals, could form through numerous feasible mechanisms. Though the presence of N-heterocycles such as pyrrole is unconfirmed in Titan’s atmosphere or the interstellar medium, photoexcitation of pyrrole leads to homolytic dehydrogenation of the apical nitrogen, leaving the ground state radical ( $A^\bullet$ ). Radiative electron attachment to this species, which has a high electron affinity, would result in the aromatic ( $A^-$ ).

Other pathways, such as cyclization reactions between CN and propyne, could similarly lead to ( $A^-$ ) or ( $A^\bullet$ ). We found that one such pathway involving  $CN^-$  was not particularly feasible, as it passed through high energy transition states and intermediates over the course of cyclization. However, a similar reaction involving *radical*  $CN^\bullet$  was not hindered in this way. All barriers were submerged beneath the energy of reactants for the radical pathway leading to ( $A^\bullet$ ), indicating that formation of this heterocycle could occur without outside energetic input in cold extraterrestrial environments.

( $F^+$ ), the minimum-energy isomer of  $C_4H_4N$  on the cationic PES, could similarly form via many routes. Ion-neutral chemistry between carbocations and small nitrogen-containing species are viable production pathways to ( $F^+$ ), as is proton attachment to allenyl cyanide.

By characterizing  $C_4H_4N$  in anionic, radical, and cationic states, we identified lowest-energy structures of each respective type that could be present in non-Earth environments. We have found that anionic ( $A^-$ ) and cationic ( $F^+$ ) isomers are global minima on their respective potential energy surfaces. Either of these species can form from reactions between smaller molecules that are readily available in some interstellar environments such as dense molecu-



lar clouds. Our work indicates that these ionic isomers of  $C_4H_4N$  may be synthesized in Titan’s atmosphere and contribute to the molecular mass data collected by the Cassini INMS. Given the reactivity of ionic species in this environment, molecules such as anionic ( $A^-$ ) and cationic ( $F^+$ ) could go on to participate in the formation of complex organics. These accurate structures, along with their ro-vibrational data (provided in the SI) may also be useful for deconvoluting extraterrestrial spectra of nitrogen-containing molecules.

Additionally, we’ve highlighted that the formation of these molecules through reactions involving radicals can pass through submerged barriers, and are thus quite feasible in cold, energy deficient environments. Radical (A), potentially formed via the radical-neutral pathway shown in Fig. 12 could have similar reactivity to its precursors and is a very interesting candidate to explore when contemplating the formation mechanisms of nitrogenated PAH.

Our results are a contribution towards better understanding species present and chemistry occurring in the atmosphere of Titan (and perhaps that of early Earth), dense molecular clouds, or other extraterrestrial sources. Further studies interrogating  $C_4H_4N$  and other nitrogen-containing ions are needed to continue to probe the composition and chemistry of Titan’s atmosphere and beyond.

## Acknowledgements

This material is based upon work supported by the National Aeronautics and Space Administration through the NASA Astrobiology Institute under Cooperative Agreement Notice NNH13ZDA017C issued through the Science Mission Directorate.

Special thanks to the NASA Ames ARC NAI CAN-7 team for support and inclusion.

## Supplementary Information

Molecular geometries for all molecules mentioned here are available in the SI document online. As indicated in the text, the SI also contains vibrational constants and IR intensities, as well as a comparison between CCSD(T)/CBS and DFT (using  $\omega B97X-V/aug-cc-pVTZ$ ) for calculated isomer energetics.

## References

- (1) Miller, S. L.; Urey, H. C. Organic Compound Synthesis on the Primitive Earth. *Science* **1959**, *130*, 245–251.
- (2) Strecker, A. Ueber die künstliche Bildung der Milchsäure und einen neuen, dem Glycocoll homologen Körper;. *Justus Liebigs Ann. Chem* **1850**, *75*, 27–45.
- (3) Taillades, J.; Beuzelin, I.; Garrel, L.; Tabacik, V.; Bied, C.; Commeyras, A. N-Carbamoyl- $\alpha$ -Amino Acids Rather than Free  $\alpha$ -Amino Acids Formation in the Primitive Hydrosphere: A Novel Proposal for the Emergence of Prebiotic Peptides. *Origins of life and evolution of the biosphere* **1998**, *28*, 61–77.
- (4) Gibb, E. L.; Whittet, D. C. B.; Boogert, A. C. A.; Tielens, A. G. G. M. Interstellar Ice: The Infrared Space Observatory Legacy. *ApJS*. **2004**, *151*, 35–73.
- (5) Matthews, C.; Moser, R. E. Peptide Synthesis from Hydrogen Cyanide and Water. *Nature* **1967**, *215*, 1230–1234.
- (6) Roy, D.; Najafian, K.; von Ragué Schleyer, P. Chemical evolution: The mechanism of the formation of adenine under prebiotic conditions. *Proc. Natl. Acad. Sci.* **2007**, *104*, 17272–17277.
- (7) Ferris, J. P.; Hagan, W. J. HCN and chemical evolution: The possible role of

- cyano compounds in prebiotic synthesis. *Tetrahedron* **1984**, *40*, 1093 – 1120.
- (8) Dartnell, L. R. Ionizing Radiation and Life. *Astrobiology* **2011**, *11*, 551–582, PMID: 21774684.
  - (9) Chyba, C.; Sagan, C. Endogenous production, exogenous delivery and impact-shock synthesis of organic molecules: an inventory for the origins of life. *Nature* **1992**, *355*, 125–132.
  - (10) Zamirri, L.; Ugliengo, P.; Ceccarelli, C.; Rimola, A. Quantum Mechanical Investigations on the Formation of Complex Organic Molecules on Interstellar Ice Mantles. Review and Perspectives. *ACS Earth Space Chem.* **2019**, *3*, 1499–1523.
  - (11) Saladino, R.; Dia Mauro, E.; Garcia-Ruiz, J. M. A Universal Geochemical Scenario for Formamide Condensation and Prebiotic Chemistry. *Chem. Eur. J.* **2019**, *25*, 3181–3189.
  - (12) D.E. Woon, The Astrochymist. <http://astrochymist.org/>, 2019; Online; accessed 20 November 2019.
  - (13) Kvenvolden, K.; Lawless, J.; Pering, K.; Peterson, E.; Flores, J.; Ponnamperna, C.; Kaplan, I. R.; Moore, C. Evidence for Extraterrestrial Amino-acids and Hydrocarbons in the Murchison Meteorite. *Nature* **1970**, *228*, 923–926.
  - (14) Engel, M.; Macko, S. Isotopic evidence for extraterrestrial non-racemic amino acids in the Murchison meteorite. *Nature* **1997**, *389*, 265–268.
  - (15) Engel, M.; Macko, S.; Silfer, J. Carbon isotope composition of individual amino acids in the Murchison meteorite. *Nature* **1990**, *348*, 47–49.
  - (16) Callahan, M. P.; Smith, K. E.; Cleaves, H. J.; Ruzicka, J.; Stern, J. C.; Glavin, D. P.; House, C. H.; Dworkin, J. P. Carbonaceous meteorites contain a wide range of extraterrestrial nucleobases. *Proc. Natl. Acad. Sci.* **2011**, *108*, 13995–13998.
  - (17) Bera, P.; Nuevo, M.; Milam, S.; Sandford, S.; Lee, T. Mechanism for the Abiotic Synthesis of Uracil via UV-induced Oxidation of Pyrimidine in Pure H<sub>2</sub>O Ices under Astrophysical Conditions. *J. Chem. Phys.* **2010**, *133*, 104303.
  - (18) Bera, P. P.; Nuevo, M.; Materese, C. K.; Sandford, S. A.; Lee, T. J. Mechanisms for the formation of thymine under astrophysical conditions and implications for the origin of life. *J. Chem. Phys.* **2016**, *144*, 144308.
  - (19) Bera, P. P.; Stein, T.; Head-Gordon, M.; Lee, T. J. Mechanisms of the Formation of Adenine, Guanine, and Their Analogues in UV-Irradiated Mixed NH<sub>3</sub>:H<sub>2</sub>O Molecular Ices Containing Purine. *Astrobiology* **2017**, *17*, 771–785, PMID: 28708419.
  - (20) Materese, C. K.; Nuevo, M.; Sandford, S. A. The Formation of Nucleobases from the Ultraviolet Photoirradiation of Purine in Simple Astrophysical Ice Analogues. *Astrobiology* **2017**, *17*, 761–770, PMID: 28723229.
  - (21) Sandford, S. A.; Bera, P. P.; Lee, T. J.; Materese, C. K.; Nuevo, M. The Photosynthesis and Photo-Stability of Nucleic Acids in Prebiotic Extraterrestrial Environments. *Top. Curr. Chem.* **2015**, *356*, 123–164.
  - (22) Plows, F. L.; Elsil, J. E.; Zare, R. N.; Buseck, P. R. Evidence that polycyclic aromatic hydrocarbons in two carbonaceous chondrites predate parent-body formation. *Geochim. Cosmochim. Acta* **2003**, *67*, 1429 – 1436.
  - (23) Ehrenfreund, P.; Charnley, S. B. Organic Molecules in the Interstellar Medium, Comets, and Meteorites: A Voyage from Dark Clouds to the Early Earth. *Annu. Rev. Astron. Astrophys.* **2000**, *38*, 427–483.

- (24) Alves, J. F.; Lada, C. J.; Lada, E. A. Internal structure of a cold dark molecular cloud inferred from the extinction of background starlight. *Nature* **2001**, *409*, 159–161.
- (25) Ziurys, L. M. The chemistry in circumstellar envelopes of evolved stars: Following the origin of the elements to the origin of life. *Proc. Natl. Acad. Sci.* **2006**, *103*, 12274–12279.
- (26) Parker, D. S. N.; Kaiser, R. I.; Kostko, O.; Troy, T. P.; Ahmed, M.; Sun, B.-J.; Chen, S.-H.; Chang, A. H. H. On the formation of pyridine in the interstellar medium. *Phys. Chem. Chem. Phys.* **2015**, *17*, 32000–32008.
- (27) Parker, D. S. N.; Kaiser, R. I. On the formation of nitrogen-substituted polycyclic aromatic hydrocarbons (NPAHs) in circumstellar and interstellar environments. *Chem. Soc. Rev.* **2017**, *46*, 452–463.
- (28) Kaiser, R. I.; Parker, D. S.; Mebel, A. M. Reaction Dynamics in Astrochemistry: Low-Temperature Pathways to Polycyclic Aromatic Hydrocarbons in the Interstellar Medium. *Annu. Rev. Phys. Chem.* **2015**, *66*, 43–67, PMID: 25422849.
- (29) Parker, D. S. N.; Yang, T.; Dangi, B. B.; Kaiser, R. I.; Bera, P. P.; Lee, T. J. Low temperature formation of Nitrogen-Substituted Polycyclic Aromatic Hydrocarbons (PANHs) - Barrierless Routes to Dihydroisoquinolines. *ApJ.* **2015**, *815*, 115.
- (30) Hamid, A. M.; Bera, P. P.; Lee, T. J.; Aziz, S. G.; Alyoubi, A. O.; El-Shall, M. S. Evidence for the Formation of Pyrimidine Cations from the Sequential Reactions of Hydrogen Cyanide with the Acetylene Radical Cation. *J. Phys. Chem. Lett.* **2014**, *5*, 3392–3398, PMID: 26278451.
- (31) Hamid, A. M.; El-Shall, M. S.; Hilal, R.; Elroby, S.; Aziz, S. G. Unconventional hydrogen bonding to organic ions in the gas phase: Stepwise association of hydrogen cyanide with the pyridine and pyrimidine radical cations and protonated pyridine. *J. Chem. Phys.* **2014**, *141*, 054305.
- (32) The Formation of Polycyclic Aromatic Hydrocarbons in Evolved Circumstellar Environments. 2011.
- (33) Cable, M. L.; Hörst, S. M.; Hodyss, R.; Beauchamp, P. M.; Smith, M. A.; Willis, P. A. Titan Tholins: Simulating Titan Organic Chemistry in the Cassini-Huygens Era. *Chemical Reviews* **2012**, *112*, 1882–1909, PMID: 22091924.
- (34) Brown, R. H.; Lebreton, J.-P.; Waite, J. H. *Titan from Cassini-Huygens*; Springer: New York, 2009.
- (35) Coates, A. J.; Crary, F. J.; Lewis, G. R.; Young, D. T.; Waite Jr., J. H.; Sittler Jr., E. C. Discovery of heavy negative ions in Titan’s ionosphere. *Geophys. Res. Lett.* **2007**, *34*.
- (36) Coates, A.; Wellbrock, A.; Lewis, G.; Jones, G.; Young, D.; Crary, F.; Waite, J. Heavy negative ions in Titan’s ionosphere: Altitude and latitude dependence. *Planet. Space Sci.* **2009**, *57*, 1866 – 1871.
- (37) Crary, F.; Magee, B.; Mandt, K.; Waite, J.; Westlake, J.; Young, D. Heavy ions, temperatures and winds in Titan’s ionosphere: Combined Cassini CAPS and INMS observations. *Planet. Space Sci.* **2009**, *57*, 1847 – 1856.
- (38) Cravens, T.; et al., Composition of Titan’s ionosphere. *Geophys. Res. Lett.* **2006**,
- (39) Waite, J. H. et al. Ion Neutral Mass Spectrometer Results from the First Flyby of Titan. *Science* **2005**, *308*, 982–986.
- (40) Waite, J. H.; Young, D. T.; Cravens, T. E.; Coates, A. J.; Crary, F. J.; Magee, B.; Westlake, J. The

- Process of Tholin Formation in Titan's Upper Atmosphere. *Science* **2007**, *316*, 870–875.
- (41) Cravens, T.; et al., Composition of Titan's ionosphere. *Geophys. Res. Lett.* **2006**, *33*.
- (42) Dubois, D.; Carrasco, N.; Bourgalais, J.; Vettier, L.; Desai, R. T.; Wellbrock, A.; Coates, A. J. Nitrogen-containing Anions and Tholin Growth in Titan's Ionosphere: Implications for Cassini CAPS-ELS Observations. *ApJ.* **2019**, *872*, L31.
- (43) Horvath, G.; Aranda-Gonzalvo, Y.; Mason, N. J.; Zahoran, M.; Matejcik, S., Negative ions formed in N<sub>2</sub>/CH<sub>4</sub>/Ar discharge - A simulation of Titan's atmosphere chemistry. *Eur. Phys. J. Appl. Phys.* **2010**, *49*, 13105.
- (44) Dubois, D.; Sciamma-O'Brien, E.; Fortenberry, R. C. The Fundamental Vibrational Frequencies and Spectroscopic Constants of the Dicyanoamine Anion, NCNCN<sup>-</sup> (C<sub>2</sub>N<sub>3</sub><sup>-</sup>): Quantum Chemical Analysis for Astrophysical and Planetary Environments. *ApJ.* **2019**, *883*, 109.
- (45) Motiyenko, R.; Armieieva, I.; Margulès, L.; Alekseev, E.; Guillemin, J.-C. Rotational spectroscopy of malononitrile and its corresponding monoisocyanide isomer, isocynoacetoneitrile. *Astron. Astrophys.* **2019**, *623*.
- (46) Custer, T.; Szczepaniak, U.; Gronowski, M.; Fabisiewicz, E.; Couturier-Tamburelli, I.; Kołos, R. Density Functional Exploration of C<sub>4</sub>H<sub>3</sub>N Isomers. *J. Phys. Chem. A* **2016**, *120*, 5928–5938.
- (47) Lattelais, M.; Ellinger, Y.; Matrane, A.; Guillemin, J.-C. Looking for heteroaromatic rings and related isomers as interstellar candidates. *Phys. Chem. Chem. Phys.* **2010**, *12*, 4165–4171.
- (48) Broten, N. W.; MacLeod, J. M.; Avery, L. W.; Irvine, W. M.; Hoglund, B.; Friberg, P.; Hjalmarsen, A. The detection of interstellar methylcyanoacetylene. *ApJ.* **1984**, *276*, L25–L29.
- (49) Lovas, F. J.; Remijan, A. J.; Hollis, J. M.; Jewell, P. R.; Snyder, L. E. Hyperfine Structure Identification of Interstellar Cyanoallene toward TMC-1. *ApJ.* **2006**, *637*, L37–L40.
- (50) Chin, Y.-N.; Kaiser, R. I.; Lemme, C.; Henkel, C. Detection of Interstellar Cyanoallene and its Implications for Astrochemistry. *Astrochemistry - From Laboratory Studies to Astronomical Observations*. 2006; pp 149–153.
- (51) Soorkia, S.; Taatjes, C. A.; Osborn, D. L.; Selby, T. M.; Trevitt, A. J.; Wilson, K. R.; Leone, S. R. Direct detection of pyridine formation by the reaction of CH (CD) with pyrrole: a ring expansion reaction. *Phys. Chem. Chem. Phys.* **2010**, *12*, 8750–8758.
- (52) Sah, C.; Yadav, A. K.; Venkataramani, S. Deciphering Stability of Five-Membered Heterocyclic Radicals: Balancing Act Between Delocalization and Ring Strain. *J. Phys. Chem. A* **2018**, *122*, 5464–5476, PMID: 29791155.
- (53) Holzmeier, F.; Wagner, I.; Fischer, I.; Bodi, A.; Hemberger, P. Pyrolysis of 3-Methoxypyridine. Detection and Characterization of the Pyrrolyl Radical by Threshold Photoelectron Spectroscopy. *J. Phys. Chem. A* **2016**, *120*, 4702–4710, PMID: 26698131.
- (54) Hong, X.; Zhang, L.; Zhang, T.; Qi, F. An Experimental and Theoretical Study of Pyrrole Pyrolysis with Tunable Synchrotron VUV Photoionization and Molecular-Beam Mass Spectrometry. *J. Phys. Chem. A* **2009**, *113*, 5397–5405.
- (55) Mardirossian, N.; Head-Gordon, M.  $\omega$ B97X-V: A 10-parameter, range-separated hybrid, generalized gradient

- approximation density functional with nonlocal correlation, designed by a survival-of-the-fittest strategy. *Phys. Chem. Chem. Phys.* **2014**, *16*, 9904–9924.
- (56) Mardirossian, N.; Head-Gordon, M. Exploring the limit of accuracy for density functionals based on the generalized gradient approximation: Local, global hybrid, and range-separated hybrid functionals with and without dispersion corrections. *J. Chem. Phys.* **2014**, *140*, 18A527.
- (57) Becke, A. D. Perspective: Fifty years of density-functional theory in chemical physics. *J. Chem. Phys.* **2014**, *140*, 18A301.
- (58) Goerigk, L.; Hansen, A.; Bauer, C.; Ehrlich, S.; Najibi, A.; Grimme, S. A look at the density functional theory zoo with the advanced GMTKN55 database for general main group thermochemistry, kinetics and noncovalent interactions. *Phys. Chem. Chem. Phys.* **2017**, *19*, 32184–32215.
- (59) Najibi, A.; Goerigk, L. The Nonlocal Kernel in van der Waals Density Functionals as an Additive Correction: An Extensive Analysis with Special Emphasis on the B97M-V and  $\omega$ B97M-V Approaches. *Journal of Chemical Theory and Computation* **2018**, *14*, 5725–5738, PMID: 30299953.
- (60) Gräfenstein, J.; Kraka, E.; Cremer, D. The impact of the self-interaction error on the density functional theory description of dissociating radical cations: Ionic and covalent dissociation limits. *J. Chem. Phys.* **2004**, *120*, 524–539.
- (61) Cohen, A. J.; Mori-Sánchez, P.; Yang, W. Challenges for Density Functional Theory. *Chemical Reviews* **2012**, *112*, 289–320.
- (62) Lee, T. J.; Schaefer, H. F. Systematic study of molecular anions within the self-consistent field approximation:  $\text{OH}^-$ ,  $\text{CN}^-$ ,  $\text{C}_2\text{H}^-$ ,  $\text{NH}_2^-$ , and  $\text{CH}_3^-$ . *J. Chem. Phys.* **1985**, *83*, 1784–1794.
- (63) Glendening, E.; Badenhop, J.; Karafilogou, P.; Landis, C.; Weinhold, F. NBO 7.0. Theoretical Chemistry Institute, University of Wisconsin, Madison, 2018.
- (64) Raghavachari, K.; Trucks, G.; Pople, J.; Head-Gordon, M. A fifth-order perturbation comparison of electron correlation theories. *Chem. Phys. Lett.* **1989**, *157*, 479–483.
- (65) Feyereisen, M.; Fitzgerald, G.; Komornicki, A. Use of approximate integrals in ab initio theory. An application in MP2 energy calculations. *Chem. Phys. Lett.* **1993**, *208*, 359–363.
- (66) Bernholdt, D.; Harrison, R. Large-scale correlated electronic structure calculations: The RI-MP2 method on parallel computers. *Chem. Phys. Lett.* **1996**, *250*, 477–484.
- (67) Halkier, A.; et al., Basis-set convergence in correlated calculations on Ne,  $\text{N}_2$ ,  $\text{H}_2\text{O}$ . *Chem. Phys. Lett.* **1998**, *286*, 243–252.
- (68) Behn, A.; Zimmerman, P.; Bell, A.; Head-Gordon, M. Efficient exploration of reaction paths via a freezing string method. *J. Chem. Phys.* **2011**, *135*.
- (69) Baker, J. An algorithm for the location of transition states. *J. Comput. Chem.* **1986**, *7*, 385–395.
- (70) Shao, Y. et al. Advances in molecular quantum chemistry contained in the Q-Chem 4 program package. *Molecular Physics* **2015**, *113*, 184–215.
- (71) Schofield, K. *Hetero-aromatic Nitrogen Compounds: Pyrroles and Pyridines*; Springer Science+Business Media, LLC, 1967.

- (72) Haynes, W. M.; Lide, D. R.; Bruno, T. J. *CRC Handbook of Chemistry and Physics: A Ready-reference Book of Chemical and Physical data*; Boca Raton, Florida: CRC Press, 2016.
- (73) Katritzky, A. R.; Ramsden, C. A.; Joule, J. A.; Zhdankin, V. V. *Handbook of Heterocyclic Chemistry (3rd Edition)*; Elsevier, 2010.
- (74) Jiao, H.; Schleyer, P. v. R.; Mo, Y.; McAllister, M. A.; Tidwell, T. T. Magnetic Evidence for the Aromaticity and Antiaromaticity of Charged Fluorenyl, Indenyl, and Cyclopentadienyl Systems. *J. Am. Chem. Soc.* **1997**, *119*, 7075–7083.
- (75) Gianola, A. J.; Ichino, T.; Hoenigman, R. L.; Kato, S.; Bierbaum, V. M.; Lineberger, W. C. Thermochemistry and Electronic Structure of the Pyrrolyl Radical. *J. Phys. Chem. A* **2004**, *108*, 10326–10335.
- (76) P. F. Lee, E.; G. Wright, T. A study of the lowest-lying triplet and singlet states of the cyclopentadienyl cation ( $c\text{-C}_5\text{H}_5^+$ ). *Phys. Chem. Chem. Phys.* **1999**, *1*, 219–225.
- (77) Wiberg, K. B. Antiaromaticity in Monocyclic Conjugated Carbon Rings. *Chem. Rev.* **2001**, *101*, 1317–1332, PMID: 11710223.
- (78) Breslow, R.; Groves, J.; Ryan, G. Cyclopropenyl cation. *J. Am. Chem. Soc.* **1967**,
- (79) Byun, Y.; Saebo, S.; Pittman Jr, C. An ab initio study of potentially aromatic and antiaromatic three-membered rings. *J. Am. Chem. Soc.* **1991**,
- (80) Kokkila Schumacher, S. I. L.; Bera, P. P.; Lee, T. J. Characterization of the Azirinylium Cation and Its Isomers. *J. Phys. Chem. A* **2016**, *120*, 1275–1282.
- (81) Puzzarini, C.; Bloino, J.; Tasinato, N.; Barone, V. Accuracy and Interpretability: The Devil and the Holy Grail. New Routes across Old Boundaries in Computational Spectroscopy. *Chem. Rev.* **2019**, *119*, 8131–8191, PMID: 31187984.
- (82) Puzzarini, C.; Stanton, J. F.; Gauss, J. Quantum-chemical calculation of spectroscopic parameters for rotational spectroscopy. *Int. Rev. Phys. Chem.* **2010**, *29*, 273–367.
- (83) Richter, M. J.; Ennico, K. A.; McKelvey, M. E.; Seifahrt, A. *Proc. SPIE*; Society of Photo-Optical Instrumentation Engineers (SPIE) Conference Series; 2010; Vol. 7735; p 77356Q.
- (84) Fortenberry, R. C. Quantum astrochemical spectroscopy. *Int. J. Quantum Chem.* **2017**, *117*, 81–91.
- (85) Fortenberry, R. C.; Lee, T. J. In *Chapter Six - Computational vibrational spectroscopy for the detection of molecules in space*; Dixon, D. A., Ed.; Annu. Rep. Comput. Chem.; Elsevier, 2019; Vol. 15; pp 173 – 202.
- (86) Huang, X.; Fortenberry, R. C.; Wang, Y.; Francisco, J. S.; Crawford, T. D.; Bowman, J. M.; Lee, T. J. Dipole Surface and Infrared Intensities for the cis- and trans-HOCO and DOCO Radicals. *J. Phys. Chem. A* **2013**, *117*, 6932–6939, PMID: 23199284.
- (87) Lara, L.; Lellouch, E.; Lopez-Moreno, J.; Rodrigo, R. Vertical distribution of Titan’s atmospheric neutral constituents. *J. Geophys. Res.* **1996**, *101*, 23261–23283.
- (88) Toublanc, D.; Parisot, J.; Brillet, J.; Gautier, D.; Raulin, F.; McKay, C. Photochemical modeling of Titan’s atmosphere. *Icarus* **1995**, *113*, 2–26.
- (89) Wilson, E. H.; Atreya, S. K. Current state of modeling the photochemistry of Titan’s mutually dependent atmosphere

- and ionosphere. *J. Geophys. Res.: Planets* **2004**, *109*.
- (90) Vuitton, V.; Yelle, R.; McEwan, M. Ion chemistry and N-containing molecules in Titan's upper atmosphere. *Icarus* **2007**, *191*, 722–742.
- (91) McGuigan, M.; Waite, J.; Imanaka, H.; Sacks, R. Analysis of Titan tholin pyrolysis products by comprehensive two-dimensional gas chromatography-time-of-flight mass spectrometry. *J. Chromatogr. A* **2006**,
- (92) Gautier, T.; Carrasco, N.; Buch, A.; Szopa, C.; Sciamma-O'Brien, E.; Cernogora, G. Nitrile gas chemistry in Titan's atmosphere. *Icarus* **2011**, *213*, 625 – 635.
- (93) Blank, D.; North, S.; Lee, Y. The ultraviolet photodissociation dynamics of pyrrole. *Chemical Physics* **1994**, *187*, 35–47.
- (94) Sobolewski, A. L.; Domcke, W.; Dedonder-Lardeux, C.; Jouvet, C. Excited-state hydrogen detachment and hydrogen transfer driven by repulsive  $^1\pi\sigma^*$  states: A new paradigm for nonradiative decay in aromatic biomolecules. *Phys. Chem. Chem. Phys.* **2002**, *4*, 1093–1100.
- (95) Ashfold, M. N. R.; Cronin, B.; Devine, A. L.; Dixon, R. N.; Nix, M. G. D. The Role of  $\pi\sigma^*$  Excited States in the Photodissociation of Heteroaromatic Molecules. *Science* **2006**, *312*, 1637–1640.
- (96) Zawadzki, M. M.; Thompson, J. O. F.; Burgess, E. A.; Paterson, M. J.; Townsend, D. Time-resolved photoionization spectroscopy of mixed Rydberg-valence states: indole case study. *Phys. Chem. Chem. Phys.* **2015**, *17*, 26659–26669.
- (97) Ashfold, M. N. R.; King, G. A.; Murdock, D.; Nix, M. G. D.; Oliver, T. A. A.; Sage, A. G.  $\pi\sigma^*$  excited states in molecular photochemistry. *Phys. Chem. Chem. Phys.* **2010**, *12*, 1218–1238.
- (98) Kirkby, O. M.; Parkes, M. A.; Neville, S. P.; Worth, G. A.; Fielding, H. H. Non-radiative relaxation dynamics of pyrrole following excitation in the range 249.5–200nm. *Chem. Phys. Lett.* **2017**, *683*, 179 – 185, Ahmed Zewail (1946-2016) Commemoration Issue of Chem. Phys. Lett.
- (99) Makhov, D. V.; Saita, K.; Martinez, T. J.; Shalashilin, D. V. Ab initio multiple cloning simulations of pyrrole photodissociation: TKER spectra and velocity map imaging. *Phys. Chem. Chem. Phys.* **2015**, *17*, 3316–3325.
- (100) Roberts, G. M.; Stavros, V. G. The role of  $\pi\sigma^*$  states in the photochemistry of heteroaromatic biomolecules and their subunits: insights from gas-phase femtosecond spectroscopy. *Chem. Sci.* **2014**, *5*, 1698–1722.
- (101) Wei, J.; Kuczmann, A.; Riedel, J.; Renth, F.; Temps, F. Photofragment velocity map imaging of H atom elimination in the first excited state of pyrrole. *Phys. Chem. Chem. Phys.* **2003**, *5*, 315–320.
- (102) Roberts, G. M.; Williams, C. A.; Yu, H.; Chatterley, A. S.; Young, J. D.; Ullrich, S.; Stavros, V. G. Probing ultrafast dynamics in photoexcited pyrrole: timescales for  $^1\pi^*$  mediated H-atom elimination. *Faraday Discuss.* **2013**, *163*, 95–116.
- (103) Lippert, H.; Ritze, H.; Hertel, I.; Radloff, W. Femtosecond Time-Resolved Hydrogen-Atom Elimination from Photoexcited Pyrrole Molecules. *Chem. Phys. Chem.* **2004**, *5*, 1423–1427.
- (104) Picconi, D.; Grebenshchikov, S. Y. Photodissociation dynamics in the first absorption band of pyrrole. I. Molecular

Hamiltonian and the Herzberg-Teller absorption spectrum for the  ${}^1A_2(\sigma\pi^*) < -\tilde{\chi}A_1(\pi\pi)$  transition. *J. Chem. Phys.* **2018**, *148*, 104103.

- (105) Vuitton, V.; Lavvas, P.; Yelle, R.; Garland, M.; Wellbrock, A.; Lewis, G.; Coates, A.; Wahlund, J. Negative ion chemistry in Titan's upper atmosphere. *Planet. Space Sci.* **2009**, *57*, 1558–1572.
- (106) Agúndez, M.; Cernicharo, J.; Guélin, M.; Kahane, C.; Roueff, E.; Kłos, J.; Aoziz, F. J.; Lique, F.; Marcelino, N.; Goicoechea, J. R.; González García, M.; Gottlieb, C. A.; McCarthy, M. C.; Thaddeus, P. Astronomical identification of  $CN^-$ , the smallest observed molecular anion. *A&A* **2010**, *517*, L2.
- (107) Fuente, A.; García-Burillo, S.; Gerin, M.; Teyssier, D.; Usero, A.; Rizzo, J. R.; de Vicente, P. Photon-dominated Chemistry in the Nucleus of M82: Widespread  $HOC^+$  Emission in the Inner 650 Parsec Disk. *ApJ*. **2005**, *619*, L155–L158.
- (108) Nixon, C. A.; Jennings, D. E.; Bézard, B.; Vinatier, S.; Teanby, N. A.; Sung, K.; Ansty, T. M.; Irwin, P. G. J.; Gorius, N.; Cottini, V.; Coustenis, A.; Flasar, F. M. Detection of propene in Titan's stratosphere. *ApJ*. **2013**, *776*, L14.
- (109) Kaiser, R. I.; Balucani, N. The Formation of Nitriles in Hydrocarbon-Rich Atmospheres of Planets and Their Satellites: Laboratory Investigations by the Crossed Molecular Beam Technique. *Acc. Chem. Res.* **2001**, *34*, 699–706, PMID: 11560469.
- (110) Dobrijevic, M.; Loison, J.; Hickson, K.; Gronoff, G. 1D-coupled photochemical model of neutrals, cations and anions in the atmosphere of Titan. *Icarus* **2016**, *268*, 313 – 339.
- (111) Balucani, N.; Asvany, O.; Kaiser, R.-I.; Osamura, Y. Formation of Three  $C_4H_3N$

Isomers from the Reaction of  $CN(X^2\Sigma^+)$  with Allene,  $H_2CCCH_2(X^1-A_1)$ , and Methylacetylene,  $CH_3CCH(X^1A_1)$ : A Combined Crossed Beam and Ab Initio Study. *J. Phys. Chem. A* **2002**, *106*, 4301–4311.



”TOC Graphic”

